PERGAMON

International Journal of Solids and Structures 38 (2001) 5679–5702

INTERNATIONAL JOURNAL OF SOLIDS and STRUCTURES

www.elsevier.com/locate/ijsolstr

Spectral element modeling for the beams treated with active constrained layer damping

Usik Lee *, Joohong Kim

Department of Mechanical Engineering, Inha University, 253 Yonghyun-Dong, Nam-Ku, Inchon 402-751, South Korea

Received 10 December 1999

Abstract

This paper introduces a spectrally formulated finite element for the beams with active constrained layer damping (ACLD). The spectral ACLD beam element is formulated from exact wave solutions of a set of fully coupled dynamic equations of motion. The fully coupled dynamic equations of motion are derived by using Hamilton's principle, and they include the axial motion and rotary inertia of the viscoelastic layer. The dynamic responses obtained by the experiment, spectral element method and the finite element method are compared to evaluate the validity and accuracy of the present spectral ACLD beam element model. The control performances of an actively controlled ACLD beam predicted by using the present spectral element model and the conventional finite element model are also compared. The spectral ACLD beam element model is found to provide very reliable results when compared with the conventional finite element model. © 2001 Published by Elsevier Science Ltd.

Keywords: Spectral element method; Active constrained layer damping; Beams; Viscoelastic damping; Active control

1. Introduction

Viscoelastic materials (VEM) and piezoelectric materials (PZT) have been applied to the active control of structural vibrations and noises. They are usually bonded on the surfaces of vibrating structures. Thus, the resulting structures become the multi-layer laminate structures. There are numerous examples of beam-typed multi-layer laminate structures. They are the elastic–elastic two-layer beam (Timoshenko, 1925; Hess, 1969), elastic–VEM two-layer beam (Oberst, 1952), elastic–VEM–elastic three-layer beam (i.e. passive constrained layer damping (PCLD) (Kerwin, 1959; DiTaranto, 1965; Mead and Markus, 1969; Yan and Dowell, 1972), elastic–PZT two-layer beams (Crawley and de Luis, 1987), and the elastic–VEM–PZT three-layer beams (i.e. active constrained layer damping (ACLD)) (Plump and Hubbard, 1986; Baz, 1993; Leibowitz and Vinson, 1993; Shen, 1994; McTavish and Hughes, 1993; Lam et al., 1995; Nath and Wereley, 1995).

* Corresponding author. Tel.: +82-32-860-7318; fax: +82-32-866-1434.
E-mail addresses: ulee@dragon.inha.ac.kr, ulee@inha.ac.kr (U. Lee).

0020-7683/01/$ - see front matter © 2001 Published by Elsevier Science Ltd.
PII: S0020-7683(00)00360-7

Because of its importance in understanding the fundamental physics and design applications of multi-layered laminate beams, the development of various structural theories has received many attentions over the years. Research efforts can be distinguished on the basis of several key features such as (1) the geometric configuration and materials, (2) the assumptions underlying the governing equations, (3) the VEM damping model, and (4) the response solutions method.

Timoshenko (1925) is probably the first to derive the elasticity solutions for two-layered infinite bi-metal thermostats. Later Hess (1969) derived the elasticity solutions for two-layered finite elastic strip. After Oberst (1952) introduced the concept of free layered viscoelastic damping treatment, Kerwin (1959) developed one of the first theories for simply supported three-layered PCLD beam using complex modulus. Later DiTaranto (1965) derived the sixth-order differential equation of motion in terms of longitudinal displacement. In 1969, Mead and Markus derived the sixth-order differential equation of motion in terms of the transverse displacement for a three-layered PCLD beam. Yan and Dowell (1972) developed five governing equations by using the virtual work principle of elasticity theory. They derived a simplified fourth-order differential equation of motion.

For PZT applications to active vibration controls, Crawley and de Luis (1987) proposed the uniform strain model of static interaction between the base beam and the segmented PZT actuators. After Crawley's work, there have been many developments for the analytical and finite element models of PZT actuators/sensors. Plump and Hubbard (1986) developed a sixth-order governing equation for the transverse motion of a finite ACLD beam. They used a complex modulus approach to model the VEM layer. Baz (1993) proposed a new ACLD with an additional piezoelectric sensor layer between the base structure and the VEM layer, and he derived a sixth-order dynamic equation of motion based on the model of Mead and Markus (1969). Leibowitz and Vinson (1993) also formulated a sixth-order dynamic equation of motion for the three-layer ACLD beam by using an energy approach rather than the strength-of-materials approach by Mead and Markus (1969) and Yan and Dowell (1972). An eighth-order matrix differential equation of motion was developed by Shen (1994). He used the complex modulus approach to model the VEM layer. Later, Lam et al. (1995) applied the GHM damping method to Shen's model (1994). Nath and Wereley (1995) modified the analytical approach by Mead and Markus (1969) to account for the induced strain in the PZT layer and developed a sixth-order differential equation model for a fully treated beam. Liao (1997) developed a mathematical model of a beam with a partial-coverage ACLD treatment, using GHM method to model VEM behaviors. Recently, Wang and Wereley (1998) applied a progressive wave method to a cantilevered ACLD beam. They derived a matrix equation in frequency domain by using the sixth-order differential equation of motion developed by Mead and Markus (1969).

Despite numerous analytical models of multi-layer beams, some models are not appropriate for practical use. This is in part due to the strict assumptions underlying the governing equations and in part due to the complexity of mathematical representation. Thus, there also have been developed many finite element models for ACLD beams (e.g. Lesieutre and Lee, 1996). The finite element method (FEM) can provide more realistic dynamic behavior by removing some strict assumptions that are inevitable for deriving analytical models. However, as a drawback of FEM, it is well known that a large number of finite elements should be used to obtain reliable solutions, especially at high frequency. Furthermore, the modal analysis approach commonly used in conjunction with FEM is usually limited to the low frequency regime where the relative spacing of natural frequencies is large compared to the relative parameter uncertainty. Thus, alternatives to FEM have been considered by many researchers.

In the literature, Doyle (1988) introduced the spectrally formulated finite element (simply, spectral element) to study the wave propagation in structures. In contrast to the conventional finite element, the spectral element treats the mass distribution exactly by using exact shape functions and thus provides very accurate dynamic characteristics of a structure. The spectral element matrix is the same as the exact dynamic stiffness matrix in nature (Leung, 1993; Banerjee, 1997). A structure can be discretized into many spectral elements and then they can be assembled in a completely analogous way to that used for FEM. The

FFT and inverse FFT algorithms are utilized in the solution process of spectral element analysis. This solution approach is known as the spectral element method (SEM) and it is well known to provide *exact* solutions even at high frequency as far as the structural model is valid. The SEM has been extended and applied to many problems by Lee and his colleagues (1997–1999, 2000a).

Despite the outstanding features of SEM, there have been very few applications to the multi-layer structures. This is probably due to the difficulty in obtaining the exact shape functions (which are required to formulate the spectral element) for such complex structures. In the literature, Leung and Zhou (1996) derived the dynamic stiffness matrix for the laminated composite plate based on the effective single layered plate model. However, to the author's knowledge, there have been very few spectral element applications to ACLD structures. Lee and Kim (2000b) may be the first to develop the spectral element for the elastic–PZT two-layer beams based on a set of axial-bending coupled equations of motion.

Hence, the purposes of this paper are: (1) to introduce a set of coupled equations of motion for ACLD beams, (2) to formulate spectral ACLD beam element, (3) to evaluate the validity and accuracy of the spectral ACLD beam element, and (4) to compare the control performances of an active ACLD beam predicted by SEM and FEM.

2. Coupled dynamic equations of motion

The geometry and deformation of an ACLD beam of length L is shown in Fig. 1. A set of axial-bending-shear coupled equations of motion for the ACLD beam are derived based on the following assumptions:

The shear deformations in both elastic and piezoelectric layers are negligible.
The rotary inertia is considered only for VEM layer.
Longitudinal motions are considered for all three layers.
The transverse displacement $w(x,t)$ is same for all three layers.
There is perfect continuity, but no slip, at the interfaces.
Linear theories of elasticity and piezoelectricity are applicable.
The applied voltage is uniform along the beam.
The density and thickness are uniform over the beam.

The above assumptions have been widely used in the literature (e.g. Liao, 1997), except for the assumptions (b) and (c) newly added for VEM layer in this paper.

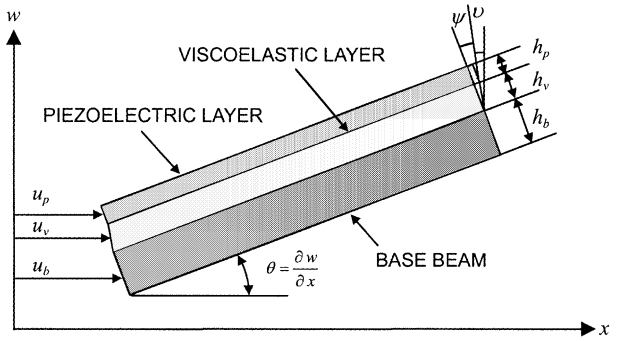

Fig. 1. The geometry and deformations of an ACLD beam.

In Fig. 1, u_b, u_v and u_p are the axial displacements of the neutral axis of the base beam, VEM layer, and the PZT layer, respectively. For perfect bonding conditions, the geometry of Fig. 1. provides the following kinematics relations:

$$\begin{aligned} u_v &= u_b - (h_b + h_v)\theta/2 + h_v\psi/2 \\ u_p &= u_b - (h_b + 2h_v + h_p)\theta/2 + h_v\psi \end{aligned} \tag{1}$$

where h_b, h_v and h_p are the thickness of the base beam, VEM layer, and the PZT layer, respectively. $\theta = \partial w/\partial x$ is the rotational angle of the base beam and ψ is the shear angle of VEM layer. As used in Eq. (1), the subscripts b, v and p will be used in the following derivations to represent the quantities for the base beam, VEM layer, and the PZT layer, respectively.

The constitutive equation of the PZT under uni-axial loading can be written as

$$\begin{Bmatrix} \sigma \\ E \end{Bmatrix} = \begin{bmatrix} C_{11}^D & -h_{31} \\ -h_{31} & \beta_{33}^s \end{bmatrix} \begin{Bmatrix} \varepsilon \\ D \end{Bmatrix} \tag{2}$$

where σ and ε are the mechanical stress and strain in the x-direction, respectively. D is the electrical displacement (charge/area in the beam vertical direction) and E is the electrical field (voltage/length along the vertical direction). C_{11}^D is the elastic stiffness, β_{33}^S is the dielectric constant, and h_{31} is the piezoelectric constant.

For one-dimensional systems, the constitutive equation for VEM can be represented in the following Stieltjes integral form (Christensen, 1982)

$$\tau(x,t) = G \circ \psi = \int_{-\infty}^{t} G(t-\tau)\frac{\partial\psi(x,\tau)}{\partial\tau}\mathrm{d}\tau \tag{3}$$

where τ is the shear stress and $G(t)$ is the relaxation function of VEM (the stress response to a unit-step strain input). This stress relaxation represents the energy loss from VEM, hence damping. In frequency domain, Eq. (3) can be rewritten in terms of the complex modulus as follows:

$$G \circ \psi = G^*(\mathrm{i}\omega)\Psi \tag{4}$$

where $G^*(\mathrm{i}\omega)$ is the complex modulus and Ψ is the spectral component defined in Eq. (18).

In most of previous works on ACLD beams, the electrical displacement through the thickness has been assumed constant whereas the inplane electric fields have been neglected. However, very recently, Cheng et al. (1999, 2000) theoretically investigated that the inplane electric fields cannot be negligible, for two-dimensional plate structures, in the circumstance where the electrical displacements on the top and bottom surfaces are unequal. They also numerically showed that the electrical displacement D through the thickness of a semi-infinite three-layer PVDF laminate is almost uniform for the case of applied potential as far as the thickness is very small. Thus, the electrical displacement D through the thickness may be assumed constant as far as the piezoelectric layer is very thin. In this situation, the inplane electrical fields may become very small to be negligible, especially when the applied voltage is uniform along the beam, which has been assumed in this paper by following Liao (1997) and other researchers. Thus, the electrical displacement D is assumed herein constant through the thickness of thin piezoelectric layer.

Using the constitutive relations of Eqs. (2) and (3), the strain energy V, the kinetic energy T, and the virtual work δW (done by applied voltage and boundary forces) can be obtained as

$$
\begin{aligned}
V &= \frac{1}{2}\int_0^L \Big\{ E_{\mathrm{b}}A_{\mathrm{b}}u_{\mathrm{b}}'^2 + E_{\mathrm{b}}I_{\mathrm{b}}w''^2 + E_{\mathrm{v}}A_{\mathrm{v}}u_{\mathrm{v}}'^2 + E_{\mathrm{v}}I_{\mathrm{v}}(w''-\psi')^2 + A_{\mathrm{v}}(G\circ\psi)\psi + C_{11}^D A_{\mathrm{p}}u_{\mathrm{p}}'^2 \\
&\qquad + C_{11}^D I_{\mathrm{p}}w''^2 - 2A_{\mathrm{p}}h_{31}Du_{\mathrm{p}}' + A_{\mathrm{p}}\beta_{33}^S D^2 \Big\}\,\mathrm{d}x \\
T &= \frac{1}{2}\int_0^L \Big\{ \rho_{\mathrm{b}}A_{\mathrm{b}}(\dot{u}_{\mathrm{b}}^2 + \dot{w}^2) + \rho_{\mathrm{v}}A_{\mathrm{v}}(\dot{u}_{\mathrm{v}}^2 + \dot{w}^2) + \rho_{\mathrm{v}}I_{\mathrm{v}}(\dot{w}'-\dot{\psi})^2 + \rho_{\mathrm{p}}A_{\mathrm{p}}(\dot{u}_{\mathrm{p}}^2 + \dot{w}^2) \Big\}\,\mathrm{d}x \\
\delta W &= \int_0^L bV(t)\delta D\,\mathrm{d}x + \overline{N}\delta u_{\mathrm{b}}\big|_L^0 + \overline{M}\delta\theta\big|_L^0 + \overline{Q}\delta w\big|_L^0 + \overline{R}\delta\psi\big|_L^0
\end{aligned}
\tag{5}
$$

where E, I, A, b, and ρ (for each layer) are the Young's modulus, area moment of inertia about the neutral axis, cross-sectional area, width, and the mass density, respectively. $\overline{N}$, $\overline{Q}$, $\overline{M}$, and $\overline{R}$ represent the boundary forces and moments corresponding to u_{b}, w, θ, and ψ, respectively, and $V(t)$ is the voltage applied to the PZT layer. The prime ($'$) and the dot ($\cdot$), in the preceding equations, indicate the partial derivatives with respect to the coordinate x and time t, respectively.

Eliminate the axial displacements u_{v} and u_{p} from Eq. (5) by using Eq. (1), and apply the resulting energies into the Hamilton's principle to yield a set of axial-bending-shear coupled equations of motion as follows:

$$
\begin{aligned}
&EI_w w'''' + \rho A\ddot{w} = -\alpha\ddot{u}_{\mathrm{b}}' + \beta u''' + \gamma\ddot{w}'' - \varepsilon_1\ddot{\psi}' + \varepsilon_2\psi''' \\
&EAu_{\mathrm{b}}'' - \rho A\ddot{u}_{\mathrm{b}} = -\alpha\ddot{w}' + \beta w''' + \varepsilon_3\ddot{\psi} - \varepsilon_4\psi'' \\
&EI_\psi\psi'' - \rho I\ddot{\psi} = -\varepsilon_1\ddot{w}' + \varepsilon_2 w''' + \varepsilon_3\ddot{u}_{\mathrm{b}} - \varepsilon_4 u'' + A_{\mathrm{v}}(G\circ\psi)
\end{aligned}
\tag{6}
$$

where

$$
\begin{aligned}
&\rho A = \rho_{\mathrm{b}}A_{\mathrm{b}} + \rho_{\mathrm{v}}A_{\mathrm{v}} + \rho_{\mathrm{p}}A_{\mathrm{p}}, \quad \rho I = \rho_{\mathrm{v}}I_{\mathrm{v}} + \rho_{\mathrm{v}}A_{\mathrm{v}}h_{\mathrm{v}}^2/4 + \rho_{\mathrm{p}}A_{\mathrm{p}}h_{\mathrm{v}}^2 \\
&\alpha = \rho_{\mathrm{v}}A_{\mathrm{v}}h_1/2 + \rho_{\mathrm{p}}A_{\mathrm{p}}h_2/2, \quad \beta = E_{\mathrm{p}}A_{\mathrm{v}}h_1/2 + E_{\mathrm{p}}A_{\mathrm{p}}h_2/2 \\
&\gamma = \rho_{\mathrm{v}}I_{\mathrm{v}} + \rho_{\mathrm{v}}A_{\mathrm{v}}h_1^2/4 + \rho_{\mathrm{p}}A_{\mathrm{p}}h_2^2/4 \\
&EA = E_{\mathrm{b}}A_{\mathrm{b}} + E_{\mathrm{v}}A_{\mathrm{v}} + E_{\mathrm{p}}A_{\mathrm{p}}, \quad E_{\mathrm{p}} = C_{11}^D - h_{31}^2/\beta_{33}^S \\
&EI_\psi = E_{\mathrm{v}}I_{\mathrm{v}} + E_{\mathrm{v}}A_{\mathrm{v}}h_{\mathrm{v}}^2/4 + E_{\mathrm{p}}A_{\mathrm{p}}h_{\mathrm{v}}^2, \quad EI_w = E_{\mathrm{b}}I_{\mathrm{b}} + E_{\mathrm{v}}I_{\mathrm{v}} + C_{11}^D I_{\mathrm{p}} + E_{\mathrm{p}}A_{\mathrm{p}}h_2^2/4 \\
&\varepsilon_1 = \rho_{\mathrm{v}}I_{\mathrm{v}} + \rho_{\mathrm{v}}A_{\mathrm{v}}h_{\mathrm{v}}h_1/4 + \rho_{\mathrm{p}}A_{\mathrm{p}}h_{\mathrm{v}}h_2/2, \quad \varepsilon_2 = E_{\mathrm{v}}I_{\mathrm{v}} + E_{\mathrm{v}}A_{\mathrm{v}}h_{\mathrm{v}}h_1/4 + E_{\mathrm{p}}A_{\mathrm{p}}h_{\mathrm{v}}h_2/2 \\
&\varepsilon_3 = \rho_{\mathrm{v}}A_{\mathrm{v}}h_{\mathrm{v}}/2 + \rho_{\mathrm{p}}A_{\mathrm{p}}h_{\mathrm{v}}, \quad \varepsilon_4 = E_{\mathrm{v}}A_{\mathrm{v}}h_{\mathrm{v}}/2 + E_{\mathrm{p}}A_{\mathrm{p}}h_{\mathrm{v}} \\
&h_1 = h_{\mathrm{b}} + h_{\mathrm{v}}, \quad h_2 = h_{\mathrm{b}} + 2h_{\mathrm{v}} + h_{\mathrm{p}}
\end{aligned}
\tag{7}
$$

The boundary conditions are obtained as the accompanying outputs from the Hamilton's principle, as

$$
\begin{aligned}
&N = \overline{N} + \overline{N}^{\mathrm{p}} \ \text{ or } \ u_{\mathrm{b}} = \overline{u}_{\mathrm{b}}, \qquad M = \overline{M} - \overline{M}^{\mathrm{p}} \ \text{ or } \ \theta = \overline{\theta} \\
&R = \overline{R} + \overline{R}^{\mathrm{p}} \ \text{ or } \ \psi = \overline{\psi}, \qquad Q = \overline{Q} \ \text{ or } \ w = \overline{w}
\end{aligned}
\tag{8}
$$

where N, M, Q and R are the resultant internal forces and moments defined in terms of displacement fields as follows:

$$
\begin{aligned}
&N = EAu_{\mathrm{b}}' - \beta w'' + \varepsilon_4\psi', \qquad Q = -EI_w w''' - \alpha\ddot{u}_{\mathrm{b}} + \beta u_{\mathrm{b}}'' + \gamma\ddot{w}' - \varepsilon_1\ddot{\psi} + \varepsilon_2\psi'' \\
&M = EI_w w'' - \beta u_{\mathrm{b}}' - \varepsilon_2\psi', \qquad R = EI_\psi\psi' - \varepsilon_2 w'' + \varepsilon_4 u_{\mathrm{b}}'
\end{aligned}
\tag{9}
$$

In Eq. (8), $\overline{N}$, $\overline{M}$, $\overline{Q}$ and $\overline{R}$ are the resultant external forces and moments applied at boundaries, and $\overline{w}$, $\overline{u}_{\mathrm{b}}$, $\overline{\theta}$ and $\overline{\psi}$ are the displacements and slopes specified at the boundaries. $\overline{N}^{\mathrm{p}}$, $\overline{M}^{\mathrm{p}}$ and $\overline{R}^{\mathrm{p}}$ are the piezoelectric

forces and moments piezoelectrically generated by the driving voltage $V(t)$ applied to PZT layer. They are given by

$$\overline{N}^{\mathrm{p}} = bd_{31}E_{\mathrm{p}}V(t), \qquad \overline{M}^{\mathrm{p}} = bd_{31}E_{\mathrm{p}}h_2V(t)/2, \qquad \overline{R}^{\mathrm{p}} = bd_{31}E_{\mathrm{p}}h_{\mathrm{v}}V(t) \tag{10}$$

By simply removing all VEM related terms (i.e. ε_1, ε_2, ε_3 and ε_4), Eq. (6) can be readily reduced to the governing equations of motion for the elastic-PZT two-layer beam (Lee and Kim, 1998).

3. Formulation of spectral ACLD beam element

The spectral ACLD beam element is formulated from the general solutions of Eq. (6). The general solutions are assumed in the spectral representations as

$$\begin{aligned} w(x,t) &= \sum_{n}^{N} W_n(x,\omega_n)\mathrm{e}^{\mathrm{i}\omega_n t} \\ u_{\mathrm{b}}(x,t) &= \sum_{n}^{N} U_n(x,\omega_n)\mathrm{e}^{\mathrm{i}\omega_n t} \\ \psi(x,t) &= \sum_{n}^{N} \Psi_n(x,\omega_n)\mathrm{e}^{\mathrm{i}\omega_n t} \end{aligned} \tag{11}$$

where W_n, U_n and Ψ_n are the spatially dependent Fourier coefficients (or spectral components) of the flexural, axial, and shear deformations, respectively. For shorthand, the subscript n used in the preceding equations will be omitted in the following.

Substituting Eq. (11) into Eq. (6) and canceling out the common time-dependent terms yields three coupled ordinary differential equations for W, U, and Ψ as

$$\begin{aligned} &EI_w W'''' - \omega^2\rho A W = \omega^2\left(\alpha U' - \gamma W'' + \varepsilon_1\Psi'\right) + \beta U''' + \varepsilon_2\Psi''' \\ &EAU'' + \omega^2\rho A U = \omega^2\left(\alpha W' - \varepsilon_3\Psi\right) + \beta W''' - \varepsilon_4\Psi'' \\ &EI_\psi\Psi'' + \omega^2\rho I\Psi = \omega^2\left(\varepsilon_1 W' - \varepsilon_3 U''\right) + \varepsilon_2 W''' - \varepsilon_4 U'' + A_{\mathrm{v}}G^*\Psi \end{aligned} \tag{12}$$

The general solutions for W, U, and Ψ can be obtained in the forms

$$\begin{aligned} W(x,\omega) &= \sum_{i=1}^{8} A_i\mathrm{e}^{k_i x} \\ U(x,\omega) &= \sum_{i=1}^{8} B_i\mathrm{e}^{k_i x} \\ \Psi(x,\omega) &= \sum_{i=1}^{8} C_i\mathrm{e}^{k_i x} \end{aligned} \tag{13}$$

where k_i $(i = 1, 2, 3, \ldots, 8)$ are the wave numbers and they are determined from the dispersion relation:

$$a_1k^8 + a_2k^6 + a_3k^4 + a_4k^2 + a_5 = 0 \tag{14}$$

where

$$
\begin{aligned}
a_1 &= EI_uEI_wEI_\psi - \varepsilon_4^2EI_w + 2\beta\varepsilon_2\varepsilon_4 - EA\varepsilon_2^2 - EI_\psi\beta^2 \\
a_2 &= \omega^2(-\rho I\beta^2 + 2\beta\varepsilon_1\varepsilon_4 - \gamma\varepsilon_4^2 + \rho IEAEI_w - 2EI_w\varepsilon_3\varepsilon_4 - 2EA\varepsilon_1\varepsilon_2 \\
&\quad + 2\beta\varepsilon_2\varepsilon_3 + 2\alpha\varepsilon_2\varepsilon_4 - \rho A\varepsilon_2^2 + \varepsilon EAEI_\psi - 2\alpha\beta EI_\psi + \rho AEI_wEI_\psi) + \mathrm{i}\omega A_\mathrm{v}G^*(\omega)\left(EAEI_w - \beta^2\right) \\
a_3 &= \omega^4\left(\rho IEI_u\gamma - \varepsilon_1^2EA + 2\beta\varepsilon_3\varepsilon_1 - 2\rho I\alpha\beta - 2\gamma\varepsilon_1\varepsilon_4 + 2\alpha\varepsilon_1\varepsilon_4 - \varepsilon_3^2EA\right. \\
&\quad \left. + \rho A\rho IEI_w + 2\alpha\varepsilon_2\varepsilon_3 - 2\rho A\varepsilon_1\varepsilon_2 - \alpha^2EI_\psi + \rho AEI_\psi\gamma\right) \\
&\quad + \mathrm{i}\omega^3A_\mathrm{v}G^*(\omega)\left(\gamma EA - 2\alpha\beta + \rho AEI_w\right) + \omega^2\left(\rho A\varepsilon_4^2 - \rho AEAEI_\psi\right) \\
a_4 &= \omega^6\left(2\alpha\varepsilon_1\varepsilon_3 - \varepsilon_3^2\gamma - \rho A\varepsilon_1^2 + \alpha^2\rho I + \gamma\rho A\rho I\right) + \omega^4\left(2\rho A\varepsilon_3\varepsilon_4 - \rho A\rho IEA - \rho I^2EI_\psi\right) \\
&\quad + \mathrm{i}\omega^5A_\mathrm{v}G^*(\omega)\left(\rho A\gamma - \alpha^2\right) - \mathrm{i}\omega^3\rho AEAA_\mathrm{v}G^*(\omega) \\
a_5 &= \omega^6\left(\rho A\varepsilon_3^2 - \rho A^2\rho I\right) - \mathrm{i}\omega^5\rho A^2A_\mathrm{v}G^*(\omega)
\end{aligned}
\tag{15}
$$

In Eq. (15), the complex modulus G^* can be expressed by either the analytical representation introduced by Soovere and Drake (1985):

$$
G^* = G_e + \frac{G_1}{1 + c_1(\mathrm{i}f_R/f_1)^{-\beta_2} + (\mathrm{i}f_R/f_1)^{-\beta_1}} \tag{16}
$$

or the GHM representation (McTavish and Hughes, 1993) :

$$
G^* = \kappa\left[1 + \sum_{r=1}^{R}\alpha_r\frac{s^2 + 2\hat{\xi}_r\hat{\omega}_r s}{s^2 + 22\hat{\xi}_r\hat{\omega}_r s + \hat{\omega}_r^2}\right] \tag{17}
$$

The parameters appeared Eqs. (16) and (17) are determined to fit the experimentally measured frequency-dependent damping data. The accuracy of the GHM model may depend on the number of dissipation variables, R. The one-term GHM model considered in this paper for the illustrative examples has a single internal dissipation coordinate, i.e. $R = 1$.

Since the dispersion defines the relationship between wave number and frequency, Eq. (14) yields eight values of wave number k at a specified frequency ω, but they always appear as $\pm$ pairs. Thus, the general solutions of Eq. (13) can be rewritten as

$$
\begin{aligned}
W(x,\omega) &= \sum_{i=1}^{4}\left(A_i\mathrm{e}^{k_ix} + A_{2i}\mathrm{e}^{-k_ix}\right) = \{\Phi(x)\}^\mathrm{T}\{\boldsymbol{A}\} \\
U(x,\omega) &= \sum_{i=1}^{4}\left(B_i\mathrm{e}^{k_ix} + B_{2i}\mathrm{e}^{-k_ix}\right) = \{\Phi(x)\}^\mathrm{T}\{\boldsymbol{B}\} \\
\Psi(x,\omega) &= \sum_{i=1}^{4}\left(C_i\mathrm{e}^{k_ix} + C_{2i}\mathrm{e}^{-k_ix}\right) = \{\Phi(x)\}^\mathrm{T}\{\boldsymbol{C}\}
\end{aligned}
\tag{18}
$$

where

$$
\begin{aligned}
\{\Phi(x)\} &= \left\{\mathrm{e}^{k_1x} \quad \mathrm{e}^{-k_1x} \quad \mathrm{e}^{k_2x} \quad \mathrm{e}^{-k_2x} \quad \mathrm{e}^{k_3x} \quad \mathrm{e}^{-k_3x} \quad \mathrm{e}^{k_4x} \quad e^{-k_4x}\right\}^\mathrm{T} \\
\{\boldsymbol{A}\} &= \left\{A_1 \quad A_2 \quad A_3 \quad A_4 \quad A_5 \quad A_6 \quad A_7 \quad A_8\right\}^\mathrm{T} \\
\{\boldsymbol{B}\} &= \left\{B_1 \quad B_2 \quad B_3 \quad B_4 \quad B_5 \quad B_6 \quad B_7 \quad B_8\right\}^\mathrm{T} \\
\{\boldsymbol{C}\} &= \left\{C_1 \quad C_2 \quad C_3 \quad C_4 \quad C_5 \quad C_6 \quad C_7 \quad C_8\right\}^\mathrm{T}
\end{aligned}
\tag{19}
$$

Substitute Eq. (18) into Eq. (12) to obtain the relations between coefficients A_I, B_i and C_I:

$$\begin{aligned} \{\boldsymbol{B}\} &= [\text{diagonal}(\lambda_i)]\{\boldsymbol{A}\} \\ \{\boldsymbol{C}\} &= [\text{diagonal}(\mu_i)]\{\boldsymbol{A}\} \end{aligned} \tag{20}$$

where

$$\begin{aligned} \lambda_i &= (-1)^i[(\beta\varepsilon_2 - EI_w\varepsilon_4)k_i^6 + \omega^2(\beta\varepsilon_1 - \alpha\varepsilon_2 - EI_w\varepsilon_3 - \gamma\varepsilon_4)k_i^4 \\ &\quad + \{(\alpha\varepsilon_1 - \gamma\varepsilon_3)\omega^4 + \rho A\varepsilon_4\omega^2\}k_i^2 + \rho A\varepsilon_3\omega^4]/\Delta_i \\ \mu_i &= (-1)^i[(EAEI_w - \beta^2)k_i^6 + \omega^2(EA\gamma + \rho AEI_w - 2\alpha\beta)k_i^4 \\ &\quad - \{(\alpha^2 - \gamma\rho A)\omega^4 + \rho AEA\omega^2\}k_i^2 - \rho A^2\omega^4]/\Delta_i \\ \Delta_i &= \{(EA\varepsilon_2 - \beta\varepsilon_4)k_i^4 + \omega^2(EA\varepsilon_1 + \rho A\varepsilon_2 - \beta\varepsilon_3 - \alpha\varepsilon_4)k_i^2 + \omega^4(\rho A\varepsilon_1 - \alpha\varepsilon_3)\}k_i \end{aligned} \tag{21}$$

By substituting Eq. (20) into Eq. (18), $W(x)$ and $\Psi(x)$ can be expressed only in terms of A_i. The coefficients A_i are first determined by applying Eq. (18), all expressed in terms of A_i, into appropriate boundary conditions. Thereafter, the other coefficients B_i and C_i can be determined from Eq. (20). The functions $\lambda_i(x)$ and $\mu_i(x)$ in Eq. (20) indicate the degree of coupling strength between axial, bending, and shear deformations. Infinite or zero values of $\lambda_i(x)$ and $\mu_i(x)$ simply imply the complete de-coupling.

By using Eq. (18), the spectral nodal displacements defined in Fig. 2 can be expressed in terms of A_i as

$$\{\boldsymbol{y}\} = [\boldsymbol{P}]\{\boldsymbol{A}\} \tag{22}$$

where

$$\{\boldsymbol{y}\} = \{\, U_1 \quad W_1 \quad \Theta_1 \quad \Psi_1 \quad U_2 \quad W_2 \quad \Theta_2 \quad \Psi_2 \,\}^{\mathrm{T}} \tag{23}$$

and the matrix $[\boldsymbol{P}]$ is given in Appendix A. Similarly, substituting Eq. (18) into Eq. (19), the spectral nodal forces and moments defined in Fig. 2 can be expressed in terms of A_i as

$$\{\boldsymbol{f}\} = [\boldsymbol{Q}]\{\boldsymbol{A}\} \tag{24}$$

where

$$\{\boldsymbol{f}\} = \{\, \overline{N}_1 - \overline{N}^{\mathrm{p}} \quad \overline{Q}_1 \quad \overline{M}_1 + \overline{M}^{\mathrm{p}} \quad \overline{R}_1 - \overline{R}^{\mathrm{p}} \quad \overline{N}_2 + \overline{N}^{\mathrm{p}} \quad \overline{Q}_2 \quad \overline{M}_2 - \overline{M}^{\mathrm{p}} \quad \overline{R}_2 + \overline{R}^{\mathrm{p}} \,\}^{\mathrm{T}} \tag{25}$$

and the matrix $[\boldsymbol{Q}]$ is given in Appendix A. In Eq. (25), $\overline{N}^{\mathrm{p}}$, $\overline{M}^{\mathrm{p}}$ and $\overline{R}^{\mathrm{p}}$ are now given by

$$\overline{N}^{\mathrm{p}} = bd_{31}E_{\mathrm{p}}V(\omega), \qquad \overline{M}^{\mathrm{p}} = bd_{31}E_{\mathrm{p}}h_2V(\omega)/2, \qquad \overline{R}^{\mathrm{p}} = bd_{31}E_{\mathrm{p}}h_{\mathrm{v}}V(\omega) \tag{26}$$

The coefficients A_i in both Eqs. (22) and (24) can be eliminated to obtain the spectral nodal force–displacement relation as

$$\{\boldsymbol{f}\} = [\boldsymbol{Q}][\boldsymbol{P}]^{-1}\{\boldsymbol{y}\} = [\boldsymbol{s}]\{\boldsymbol{y}\} \tag{27}$$

where $[\boldsymbol{s}]$ is the frequency-dependent *spectral element matrix* for ACLD beam. Computer implementation to obtain $[\boldsymbol{s}]$ can be accomplished either numerically or algebraically. Explicit expression for $[\boldsymbol{s}]$ has only become possible due to recent advance in symbolic computing (Wolfram, 1996). Since the explicit expression is too lengthy, however it will not be listed herein.

The spectral ACLD beam elements can be assembled in a completely analogous way to that used for FEM. After applying the boundary conditions to the result, the global system dynamic equation can be reduced in the form as

$$[\boldsymbol{S}]\{\boldsymbol{Y}\} = \{\boldsymbol{F}\} \tag{28}$$

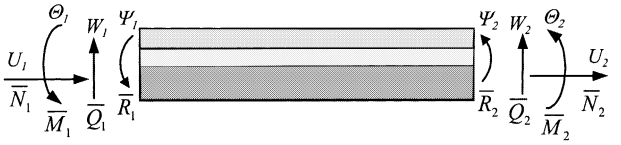

Fig. 2. Spectral element of ACLD beam.

where $[\boldsymbol{S}]$ is the global spectral matrix (or global dynamic stiffness matrix), $\{\boldsymbol{Y}\}$ the global degrees of freedom vector, and $\{\boldsymbol{F}\}$ is the global forces vector, all in frequency domain.

4. Spectral element for active ACLD beam

In the preceding section, the spectral element is formulated for the passive ACLD beam that does not include the active control law. Thus, it may be useful for the prediction of passive performance only. In order to predict the control performance of active ACLD beams, previously formulated spectral element should be modified to include the active control law. In this paper, we consider the active ACLD beam with a simple active proportional-derivative (PD) control law.

Fig. 3 shows an active ACLD beam element with a PD controller. The driving voltage applied to PZT layer is taken as the sum of two terms:

$$V(t) = -k_{\mathrm{p}} w - k_{\mathrm{d}} \dot{w} \tag{29}$$

In Eq. (29), the first term is proportional to the displacement w and the second term to the velocity $\dot{w}$, all measured at a specified location within an active ACLD beam element. k_{p} and k_{d} are the proportional and derivative gains, respectively. In frequency domain, Eq. (29) can be represented in the spectral form as

$$V(\omega) = -k_{\mathrm{p}} W - k_{\mathrm{d}}(\mathrm{i}\omega W) \tag{30}$$

By substituting Eq. (22) into Eq. (18), the flexural displacement W_0 measured at $x = x_0$ within an active ACLD beam element, for instance, can be expressed in terms of the nodal displacements vector $\{\boldsymbol{y}\}$ as follows:

$$W_0 = W(x_0, \omega) = \{\Phi(x_0)\}^{\mathrm{T}} [\boldsymbol{P}]^{-1} \{\boldsymbol{y}\} \tag{31}$$

Now, by substituting Eq. (31) into Eq. (30), the driving voltage can be rewritten in terms of the nodal displacement vector $\{\boldsymbol{y}\}$ as

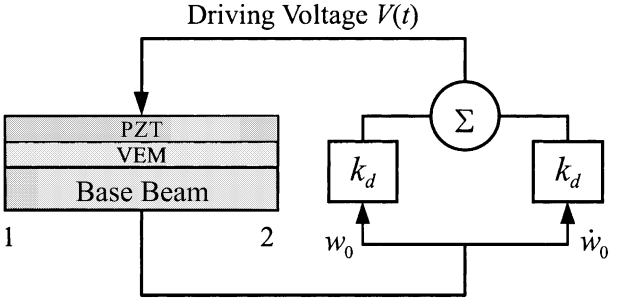

Fig. 3. An active ACLD beam element with a PD controller.

$$V(\omega) = -\left(k_{\mathrm{p}} + \mathrm{i}\omega k_{\mathrm{d}}\right)\{\Phi(x_0)\}^{\mathrm{T}}[\boldsymbol{P}]^{-1}\{\boldsymbol{y}\} \tag{32}$$

The spectral nodal forces and moments vector $\{\boldsymbol{f}\}$ defined in Eq. (24) can be split into two vectors.

$$\{\boldsymbol{f}\} = \{\boldsymbol{f}^{\mathrm{m}}\} + \{\boldsymbol{f}^{\mathrm{p}}\} \tag{33}$$

where

$$\begin{aligned} \{\boldsymbol{f}^{\mathrm{m}}\} &= \left\{ \overline{N}_1 \quad \overline{Q}_1 \quad \overline{M}_1 \quad \overline{R}_1 \quad \overline{N}_2 \quad \overline{Q}_2 \quad \overline{M}_2 \quad \overline{R}_2 \right\}^{\mathrm{T}} \\ \{\boldsymbol{f}^{\mathrm{p}}\} &= \left\{ -\overline{N}^{\mathrm{p}} \quad 0 \quad \overline{M}^{\mathrm{p}} \quad -\overline{R}^{\mathrm{p}} \quad \overline{N}^{\mathrm{p}} \quad 0 \quad -\overline{M}^{\mathrm{p}} \quad \overline{R}^{\mathrm{p}} \right\}^{\mathrm{T}} \end{aligned} \tag{34}$$

The vector $\{\boldsymbol{f}^{\mathrm{m}}\}$ contains only the external forces and moments applied at the nodes of spectral element, while the vector $\{\boldsymbol{f}^{\mathrm{p}}\}$ contains only the piezoelectrically generated forces and moments. By using Eqs. (26) and (32), the vector $\{\boldsymbol{f}^{\mathrm{p}}\}$ can be rewritten in the form

$$\{\boldsymbol{f}^{\mathrm{p}}\} = -[\boldsymbol{s}^{\mathrm{p}}]\{\boldsymbol{y}\} \tag{35}$$

where

$$\begin{aligned} [\boldsymbol{s}^{\mathrm{p}}] &= \left(k_{\mathrm{p}} + \mathrm{i}\omega k_{\mathrm{d}}\right)\{\boldsymbol{g}\}\{\boldsymbol{\Phi}(x_0)\}^{\mathrm{T}}[\boldsymbol{P}]^{-1} \\ \{\boldsymbol{g}\} &= \left\{ -\varphi \quad 0 \quad \tfrac{1}{2}h_2\varphi \quad -h_{\mathrm{v}}\varphi \quad \varphi \quad 0 \quad -\tfrac{1}{2}h_2\varphi \quad h_{\mathrm{v}}\varphi \right\}^{\mathrm{T}} \\ \varphi &= bd_{31}E_{\mathrm{p}} \end{aligned} \tag{36}$$

Substituting Eq. (33) into Eq. (27) and representing $\{\boldsymbol{f}^{\mathrm{p}}\}$ in terms of $\{\boldsymbol{y}\}$ by use of Eq. (35) yields

$$\{\boldsymbol{f}^{\mathrm{m}}\} = [\boldsymbol{s} + \boldsymbol{s}^{\mathrm{p}}]\{\boldsymbol{y}\} = [\boldsymbol{s}_{\mathrm{CONTROL}}]\{\boldsymbol{y}\} \tag{37}$$

where $[\boldsymbol{s}_{\mathrm{CONTROL}}]$ is the spectral element matrix for the active ACLD beam, in which the active PD control law is now taken into account.

5. Formulation of conventional finite element

To evaluate the accuracy of the spectral element, the conventional finite element analysis is also conducted in this study. Two VEM damping models are introduced in the preceding section. The analytical model by Soovere and Drake (1985) is not directly applicable to the time domain FEM analysis without appropriate additional efforts. However, the GHM model can be readily used in conjunction with FEM. Thus, following Liao's work (1997), the GHM model with a single internal dissipation coordinate z (i.e. one-term GHM model) is adopted herein for the conventional finite element formulation.

The displacement fields within a finite ACLD beam element are assumed in the form

$$\begin{aligned} \{\, u_{\mathrm{b}}(x) \quad w(x) \quad \theta(x) \quad \psi(x) \,\}^{\mathrm{T}} &= \left[\, \mathbf{N}_u(x) \quad \mathbf{N}_w(x) \quad \mathbf{N}'_w(x) \quad \mathbf{N}_\psi(x) \,\right]^{\mathrm{T}}\{\boldsymbol{y}_1\} \\ \{\, z(x) \,\}^{\mathrm{T}} &= \left[\, \mathbf{N}_z(x) \,\right]^{\mathrm{T}}\{\boldsymbol{y}_2\} \end{aligned} \tag{38}$$

where the shape functions matrices are defined as

$$\begin{aligned} [\boldsymbol{N}_u] &= \{\, 1-\xi \quad 0 \quad 0 \quad 0 \quad \xi \quad 0 \quad 0 \quad 0 \,\} \\ [\boldsymbol{N}_w] &= \left\{ 0 \quad 1-3\xi^2+2\xi^3 \quad L\left(\xi-2\xi^2+\xi^3\right) \quad 0 \quad 0 \quad 3\xi^2-2\xi^3 \quad L\left(-\xi^2+\xi^3\right) \quad 0 \right\} \\ \left[\boldsymbol{N}_\psi\right] &= \{\, 0 \quad 0 \quad 0 \quad 1-\xi \quad 0 \quad 0 \quad 0 \quad \xi \,\} \\ [\boldsymbol{N}_z] &= \{\, 1-\xi \quad \xi \,\} \end{aligned} \tag{39}$$

In Eq. (39), ξ is defined as x/L. The nodal DOFs vector $\{\boldsymbol{y}_1\}$ and $\{\boldsymbol{y}_2\}$ consist of eight mechanical DOFs and two internal dissipation coordinates.

Substituting the assumed displacement fields of Eq. (38) into the energy expressions of Eq. (5) and using the energy method of finite element formulation, the dynamic equation of motion (for a finite element) can be formulated in the form as

$$[\boldsymbol{M}]\{\ddot{\boldsymbol{y}}\} + [\boldsymbol{C}]\{\dot{\boldsymbol{y}}\} + [\boldsymbol{K}]\{\boldsymbol{y}\} = \{\boldsymbol{F}\} \tag{40}$$

where the vectors $\{\boldsymbol{y}\}$ and $\{\boldsymbol{F}\}$ are defined by

$$\begin{aligned} \{\boldsymbol{y}\} &= \left\{\boldsymbol{y}_1^{\mathrm{T}}; \boldsymbol{y}_2^{\mathrm{T}}\right\}^{\mathrm{T}} \\ \{\boldsymbol{F}\} &= \left\{\overline{N}_1 - \overline{N}^{\mathrm{p}} \quad \overline{Q}_1 \quad \overline{M}_1 + \overline{M}^{\mathrm{p}} \quad \overline{R}_1 - \overline{R}^{\mathrm{p}} \quad \overline{N}_2 + \overline{N}^{\mathrm{p}} \quad \overline{Q}_2 \quad \overline{M}_2 - \overline{M}^{\mathrm{p}} \quad \overline{R}_2 + \overline{R}^{\mathrm{p}}; \quad 0 \quad 0\right\}^{\mathrm{T}} \end{aligned} \tag{41}$$

and the matrices $[\boldsymbol{M}]$, $[\boldsymbol{C}]$, and $[\boldsymbol{K}]$ are the (10×10) finite element matrices into which the conventional and GHM terms are incorporated as follows:

$$\begin{aligned} [\boldsymbol{M}] &= \begin{bmatrix} \boldsymbol{M}_0 & \boldsymbol{0} \\ \boldsymbol{0} & \boldsymbol{M}_{\mathrm{G}} \end{bmatrix} \\ [\boldsymbol{C}] &= \begin{bmatrix} \boldsymbol{0} & \boldsymbol{0} \\ \boldsymbol{0} & \boldsymbol{C}_{\mathrm{G}} \end{bmatrix} \\ [\boldsymbol{K}] &= \begin{bmatrix} \boldsymbol{K}_0 & \boldsymbol{0} \\ \boldsymbol{0} & \boldsymbol{K}_{\mathrm{G}} \end{bmatrix} + [\boldsymbol{K}_{\mathrm{C}}] \end{aligned} \tag{42}$$

where $[\boldsymbol{M}_0]$ and $[\boldsymbol{K}_0]$ are the (8×8) conventional finite element mass and stiffness matrices without the damping effects of viscoelastic layer, and $[\boldsymbol{M}_{\mathrm{G}}]$, $[\boldsymbol{C}_{\mathrm{G}}]$, and $[\boldsymbol{K}_{\mathrm{G}}]$ are the (2×2) matrices augmented via the two internal dissipation coordinates. Finally, $[\boldsymbol{K}_{\mathrm{C}}]$ is the (10×10) matrix representing the coupling between the mechanical DOFs and the internal dissipation coordinates. These matrices are all tabulated in Appendix B.

6. Illustrative examples

In order to evaluate the validity and accuracy of the spectral ACLD beam element formulated herein, two types of cantilevered ACLD beams are considered as the illustrative examples. One is the patched ACLD beam that has a VEM–PZT patch bonded on the base beam as shown in Fig. 4. This patched ACLD beam is the same beam with which Liao (1997) conducted the vibration tests to measure the frequency responses as well as the FEM analysis. The other one is the uniform ACLD beam that is fully covered with VEM–PZT layer from the root to the free-end of base beam. They are made of the same materials: PKI 502 for PZT layers and 3M ISD 112 for VEM layers. They also have the same geometry, except for the length of VEM–PZT layers laminated over the same base beam. The length, width, and height of the base beam are 261.6, 12.7, and 2.286 mm, respectively. For the patched ACLD beam, a VEM–PZT patch of length 101.6 mm is bonded at 27 mm distance from the root of base beam. The geometry and material properties are further detailed in Fig. 4.

The SEM analysis and the FEM analysis are conducted for both ACLD beams. Since the SEM is developed in the frequency domain, the measured frequency-dependent complex shear modulus can be directly used in conjunction with SEM without approximation. Accordingly, both the analytical model represented by Eq. (13) and the GHM model can be also readily used in conjunction with SEM. However, it is not easy to use the frequency-dependent complex shear modulus directly in conjunction with the conventional FEM without appropriate additional efforts. This is why the GHM method was developed for the use in conjunction with FEM. In this paper, the high accuracy of the spectral ACLD beam model will be verified by comparing SEM results with FEM results. For the meaningful comparison between SEM and

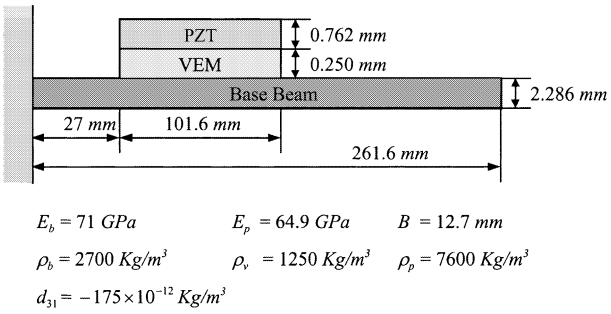

Fig. 4. Geometry and material properties of a patched ACLD beam.

FEM results, the same damping representation of viscoelastic layer should be used for both SEM and FEM models. Thus, since only the GHM model can be used in conjunction with FEM, the one-term GHM model represented by Eq. (16) is considered for both SEM and FEM models, just for the meaningful comparison between SEM and FEM results. It has been well proved that only a single spectral element is enough for the uniform structural member, regardless of its length, to obtain its accurate dynamic characteristics (Doyle, 1988; Leung, 1993). Thus, for SEM, total three spectral elements are used for the patched ACLD beam and a single spectral element for the uniform ACLD beam. However, for the conventional finite element analysis, the total number of conventional finite elements is increased until we obtain the results sufficiently converged to certain values.

To verify the validity of the present spectral ACLD beam element formulation, first the frequency response function (FRF) experimentally measured by Liao (1997) is compared in Fig. 5 with those predicted by both SEM and FEM. The ACLD beam is excited by the piezoelectric actuator with white noise input, and the FRFs in Fig. 5 are defined as the frequency responses of the displacement over input voltage, at 2 mm from the free end. A couple of peaks appeared in the measured FRF at about 80 and 120 Hz seems to be related to electrical signals (Liao, 2000). The thin solid line represents the FRF

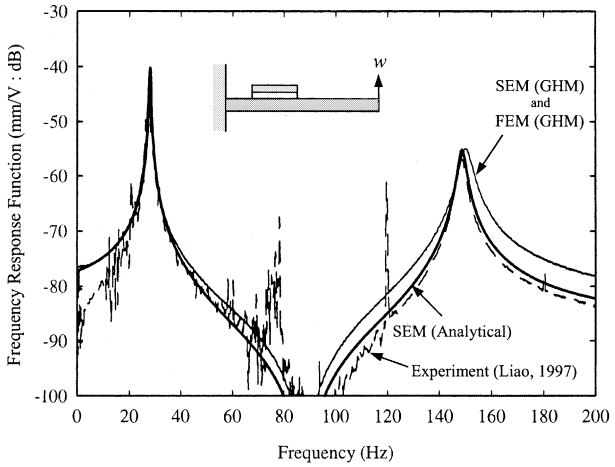

Fig. 5. Comparison of the FRFs of a patched ACLD beam obtained by the analytical model-based SEM, the one-term GHM model-based FEM, and the experiment (Liao, 1997).

obtained by the one-term GHM model-based SEM. Since a sufficient number of finite elements are used for the one-term GHM model-based FEM, the FRF by FEM is not well distinguishable from the FRF by SEM, as illustrated in Fig. 5. The thick solid line represents the FRF obtained by the analytical model-based SEM. As expected, Fig. 5 shows that the analytical model-based SEM provides the FRF that is in better agreement with measured FRF when compared with one-term GHM model-based SEM. This implies that a single internal dissipation coordinate is not enough for the GMH model to accurately represent the damping characteristics of the VEM layer. Thus, it is required for the GHM model-based SEM to take into account more internal dissipation coordinates to obtain the results further improved toward the measured FRF. Since the SEM is developed in the frequency domain, anyhow, one does not need to use any approximated model such as the GHM model in conjunction with SEM. From Fig. 5, one may expect that the direct use of the frequency-dependent complex shear modulus, rather than the use of analytical model or GHM model, in conjunction with SEM will provide the result further improved toward the measurement.

To evaluate the accuracy of the present spectral ACLD beam element model, the natural frequencies, FRFs, and the averaged errors of dynamic responses obtained by SEM are compared with those by FEM, for both patched and uniform ACLD beams. The FRFs introduced in the following are now all defined as the frequency responses of displacement over the mechanical force. The mechanical force (rectangular-type impulse force) is applied at the free end of ACLD beam for 250 μs, and the frequency response of displacement is measured at the same location.

Table 1 compares the natural frequencies of the patched ACLD beam, depending on the thickness of VEM layer. When the same one-term GHM model is applied for both SEM and FEM, table shows that the natural frequencies by FEM certainly converge to those by SEM as the total number of classical finite elements used in FEM is increased, regardless of VEM layer thickness. This may prove the well-recognized fact that SEM can provide exact solutions by using only minimum number of spectral elements (i.e. three elements for the patched ACLD beam) or degrees of freedom. Thus, in the following discussions, the results by SEM will be considered to be as the exact reference values to be compared with FEM results. The second and third columns of table compare the natural frequencies obtained by SEM using different VEM damping models. Table 1 shows that the natural frequencies are dependent of the damping models used for VEM layer. For the present example, the analytical model is found to provide a little bit lower values of

Table 1
The natural frequencies of a patched ACLD beam (n = total number of spectral elements or classical finite elements)

Modes	ω_{SEM} (Hz)		ω_{FEM} (Hz)		
	Analytical model	One-term GHM model	One-term GHM model		
	$n = 3$	$n = 3$	$n = 10$	$n = 50$	$n = 150$
When VEM layer thickness is 0.25 mm					
1st	27.882	27.879	27.923	27.898	27.897
2nd	148.539	149.791	150.677	150.067	150.045
3rd	429.694	440.596	442.779	441.098	441.039
4th	816.562	823.142	831.488	823.412	823.120
5th	1391.679	1398.595	1423.242	1399.582	1398.743
When VEM layer thickness is 0.5 mm					
1st	27.676	27.672	27.706	27.680	27.679
2nd	146.905	147.816	148.672	147.975	147.949
3rd	422.669	431.870	434.612	432.218	432.132
4th	804.272	809.850	819.938	810.197	809.835
5th	1372.590	1379.170	1408.803	1380.371	1379.326

natural frequencies when compared with the one-term GHM model. Table 1 finally shows that, in general, the natural frequencies of the patched ACLD beam decrease as the thickness of VEM layer increases.

Figs. 6 and 7 compares the FRFs obtained FEM with the exact ones by SEM for the patched ACLD beam and the uniform ACLD beam, respectively. They clearly show that the FRF by FEM gradually gets closer to the FRF by SEM as the total number of finite elements used in FEM is increased.

The errors of the dynamic responses obtained by FEM are compared in Fig. 8 for the patched ACLD beam and in Fig. 9 for the uniform ACLD beam, depending on the total number of finite elements. Since the phase difference between the dynamic responses makes it difficult to directly use the difference of dynamic response amplitudes as the error indicator, two definitions of averaged error are used in Figs. 8 and 9. One is for the errors of the peak amplitudes of dynamic response within specified time duration, and the other one is for the errors of the peak times at which the dynamic response has the peak amplitudes. In this study, the averaged errors for the first 10 peak amplitudes (i.e. $N = 10$) are obtained from

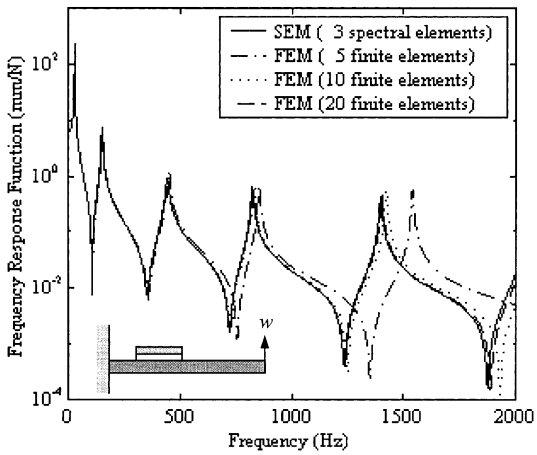

Fig. 6. Comparison of the FRFs of a patched ACLD beam obtained by SEM and FEM, all based on the one-term GHM model.

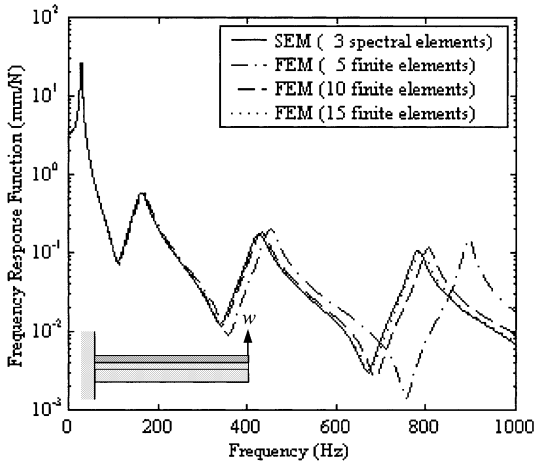

Fig. 7. Comparison of the FRFs of a uniform ACLD beam obtained by SEM and FEM, all based on the one-term GHM model.

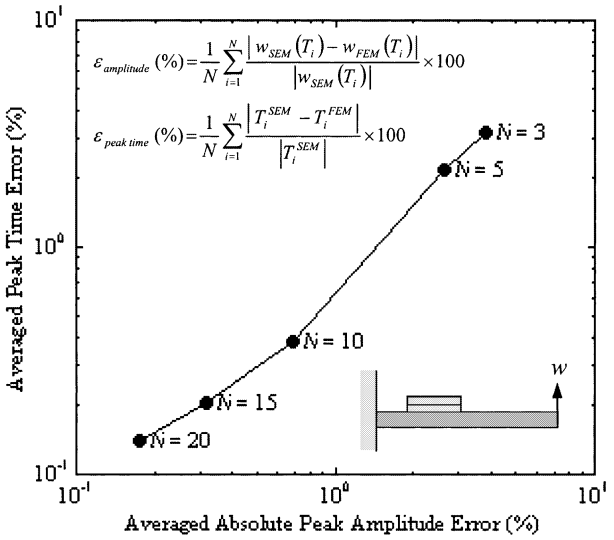

Fig. 8. Time averaged error of the dynamic responses of a patched ACLD beam obtained by FEM with respect to those by SEM (N = total number of classical finite elements used for FEM).

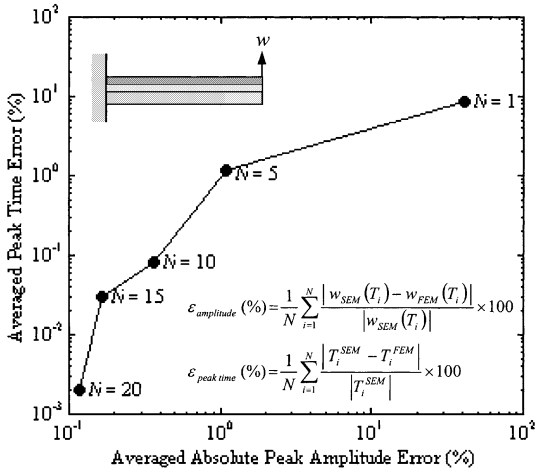

Fig. 9. Time averaged error of the dynamic responses of a uniform ACLD beam obtained by FEM with respect to those by SEM (N = total number of classical finite elements used for FEM).

$$\varepsilon_{\text{amplitude}}(\%) = \frac{1}{N}\sum_{i=1}^{N}\frac{|w_{\text{SEM}}(T_i) - w_{\text{FEM}}(T_i)|}{|w_{\text{SEM}}(T_i)|}\times 100$$
$$\varepsilon_{\text{peak time}}(\%) = \frac{1}{N}\sum_{i=1}^{N}\frac{|T_i^{\text{SEM}} - T_i^{\text{FEM}}|}{|T_i^{\text{SEM}}|}\times 100 \tag{43}$$

where w_{SEM} and w_{FEM} are the dynamic responses obtained by SEM and FEM, and T_i indicate the peak times. Figs. 8 and 9 clearly show that the errors of the dynamic responses by FEM (with respect to the exact

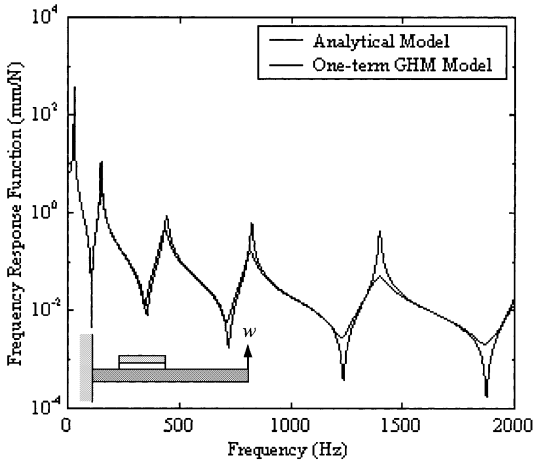

Fig. 10. Viscoelastic damping model dependence of the FRFs of a patched ACLD beam obtained by SEM.

ones by SEM) decrease as the total number of finite elements used in FEM is increased. From Figs. 8 and 9, it can be also confirmed that the patched ACLD beam requires more precise finite element discretization to meet the specified solution accuracy.

Fig. 10 compares the FRF obtained by SEM using different VEM damping models for the patched ACLD beam and Fig. 11 for the uniform ACLD beam. A single dissipation variable may not be enough for the GHM model to accurately represent the VEM layer damping. Thus, for both ACLD beams, the FRFs by one-term GHM model are found to be deviated significantly from those by the analytical model, especially at high frequency. In general, the analytical model is found to yield the FRFs of lower peaks with lower natural frequencies when compared with the one-term GHM model. The uniform ACLD beam has heavier VEM damping, thus the FRF of uniform ACLD beam is found to be much smaller than that of patched ACLD beam.

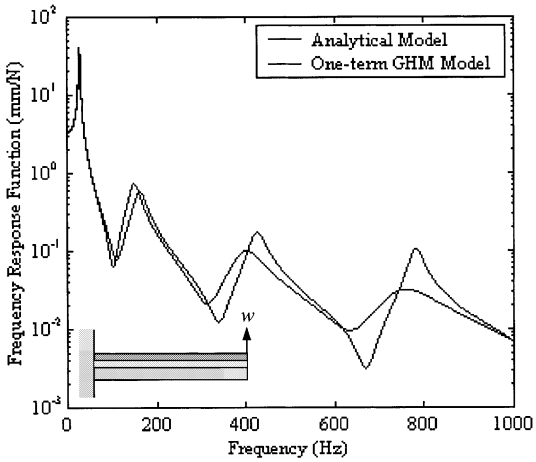

Fig. 11. Viscoelastic damping model dependence of the FRFs of a uniform ACLD beam obtained by SEM.

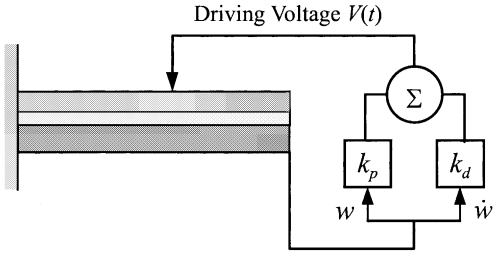

Fig. 12. An active uniform ACLD beam with a PD controller.

Lastly, the accuracy of SEM to predict the active control performance of active ACLD beams is evaluated by considering a cantilevered uniform ACLD beam with a PD controller. The active ACLD beam is shown in Fig. 12 and the control gains k_p and k_d are given by 5×10^7 V and 60 V s, respectively. Tables 2 and 3 compare the modal parameters (i.e. modal frequency and modal damping) predicted by both SEM and FEM. The active ACLD beam (i.e. controlled case) is found to have higher modal frequencies and larger modal dampings than the passive ACLD beam (i.e. uncontrolled case), which is also well illustrated in Fig. 13. Tables 2 and 3 show that the modal parameters predicted by FEM converge to those by SEM as the number of finite elements used in FEM increases. This also confirms the high accuracy of the present SEM. The FRFs and the dynamic responses for both passive and active ACLD

Table 2
Modal frequencies of the passive and active uniform ACLD beams (n = total number of spectral elements or classical finite elements)[a]

Mode	$\omega_{\text{uncontrolled}}$ (Hz)	$\omega_{\text{controlled}}$ (Hz)				
	SEM	SEM	FEM			
	$n = 1$	$n = 1$	$n = 5$	$n = 10$	$n = 20$	$n = 50$
1st	28.3	32.0	32.1	32.0	32.0	32.0
2nd	161.2	172.9	177.2	174.0	173.2	173.0
3rd	423.5	430.8	457.3	436.9	432.3	431.0
4th	780.2	785.3	898.5	808.4	790.9	786.2
5th	1240.8	1244.6	1713.1	1310.5	1260.4	1247.1

[a] Used one-term GHM model for VEM.

Table 3
Modal damping of the passive and active uniform ACLD beams (n = total number of spectral elements or classical finite elements)[a]

Mode	$\xi_{\text{uncontrolled}}$ (Hz)	$\xi_{\text{controlled}}$ (Hz)				
	SEM	SEM	FEM			
	$n = 1$	$n = 1$	$n = 5$	$n = 10$	$n = 20$	$n = 50$
1st	0.0589	0.1113	0.1119	0.1114	0.1113	0.1113
2nd	0.0830	0.0980	0.0934	0.0969	0.0978	0.0980
3rd	0.0403	0.0439	0.0365	0.0421	0.0435	0.0439
4th	0.0192	0.0203	0.0127	0.0182	0.0198	0.0202
5th	0.0095	0.0099	0.0041	0.0081	0.0094	0.0098

[a] Used one-term GHM model for VEM.

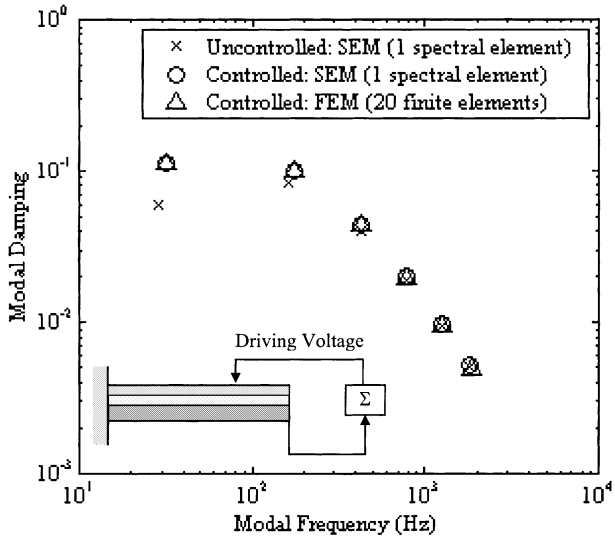

Fig. 13. Comparison of the active performances of an active uniform ACLD beam with a PD controller.

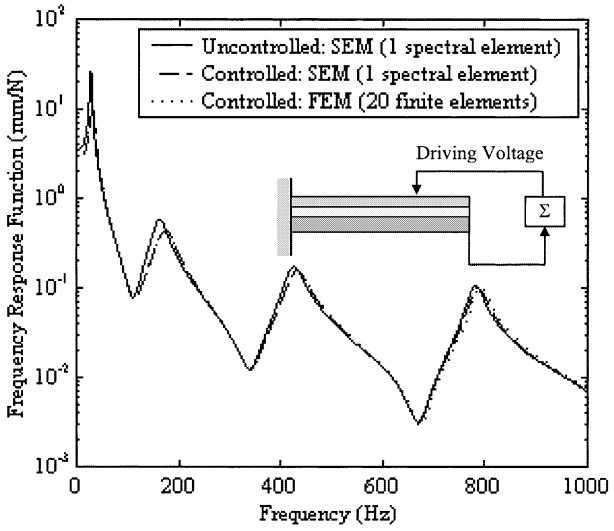

Fig. 14. Comparison of the FRFs of an active uniform ACLD beam with a PD controller.

beams are compared in Figs. 14 and 15, respectively. With the PD controller, the peaks of FRF are a little bit shifted to higher frequencies while the peak amplitudes are lowered. Accordingly, the dynamic response of active ACLD beam decays faster than the passive ACLD beam. Figs. 14 and 15 show that the FEM results (dotted lines) by using 20 finite elements are so close to the SEM results (dashed lines) that they are not almost distinguishable from each other. This also verifies that the high accuracy of SEM may be achieved by FEM only when the sufficient number of finite elements (i.e. 20 finite elements herein) is used.

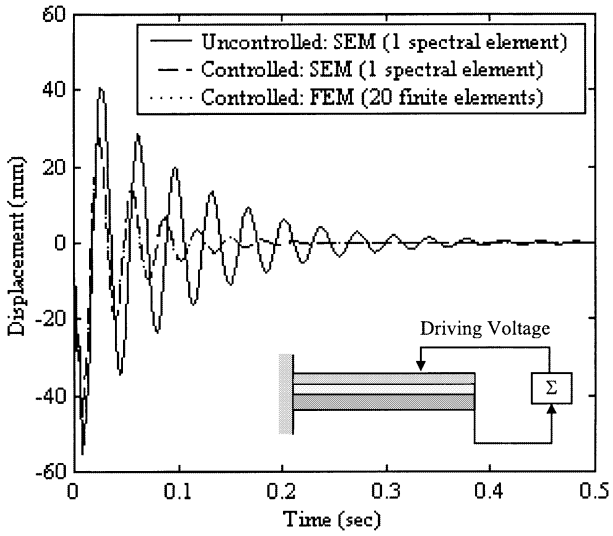

Fig. 15. Comparison of the dynamic responses of an active uniform ACLD beam with a PD controller.

7. Conclusions

In the present paper, a set of fully coupled equations of motion is derived for ACLD beams by using Hamilton's principle. The axial motion and the rotary inertia of viscoelastic layer are taken into account in the equations of motion. The SEM of ACLD beam is then formulated from the exact wave solutions of governing equations. The SEM is also developed for the ACLD beam with active control law. The frequency responses predicted by using the analytical and GHM models are compared with experimentally measured one (Liao, 1997) to observe that the use of the frequency-dependent complex shear modulus in conjunction with SEM may provide the result further improved toward the measurement. The conventional finite element model of ACLD beam is used to evaluate the accuracy of the present spectral ACLD beam model. Two types of ACLD beam are considered as the illustrative examples: the patched ACLD beam and the uniform ACLD beam. The minimum number of spectral elements is used for the SEM models: i.e., three for the patched ACLD beam and just one for the uniform ACLD beam. On the other hand, the total number of conventional finite elements used in FEM analysis is varied to observe that the FEM results indeed converge to the SEM results as the total number of conventional finite elements is increased. It is found that the SEM provides in general very accurate dynamic characteristics for both passive and active ACLD beams when compared with the conventional FEM, especially at high frequency.

Acknowledgements

This work was supported by the Brain Korea 21 Project of the Ministry of Education, Republic of Korea.

Appendix A

The matrices $[\boldsymbol{P}]$ and $[\boldsymbol{Q}]$ in Eqs. (22) and (24) are defined as follows:

$$[\boldsymbol{P}] = \begin{bmatrix} \lambda_1 & -\lambda_1 & \lambda_2 & -\lambda_2 & \lambda_3 & -\lambda_3 & \lambda_4 & -\lambda_4 \\ 1 & 1 & 1 & 1 & 1 & 1 & 1 & 1 \\ k_1 & -k_1 & k_2 & -k_2 & k_3 & -k_3 & k_4 & -k_4 \\ \mu_1 & -\mu_1 & \mu_2 & -\mu_2 & \mu_3 & -\mu_3 & \mu_4 & -\mu_4 \\ e^{Lk_1}\lambda_1 & -e^{-Lk_1}\lambda_1 & e^{Lk_2}\lambda_2 & -e^{-Lk_2}\lambda_2 & e^{Lk_3}\lambda_3 & -e^{-Lk_3}\lambda_3 & e^{Lk_4}\lambda_4 & -e^{-Lk_4}\lambda_4 \\ e^{Lk_1} & e^{-Lk_1} & e^{Lk_2} & e^{-Lk_2} & e^{Lk_3} & e^{-Lk_3} & e^{Lk_4} & e^{-Lk_4} \\ e^{Lk_1}k_1 & -e^{-Lk_1}k_1 & e^{Lk_2}k_2 & -e^{-Lk_2}k_2 & e^{Lk_3}k_3 & -e^{Lk_3}k_3 & e^{Lk_4}k_4 & -e^{-Lk_4}k_4 \\ e^{Lk_1}\mu_1 & -e^{-Lk_1}\mu_1 & e^{Lk_2}\mu_2 & -e^{-Lk_2}\mu_2 & e^{Lk_3}\mu_3 & -e^{Lk_3}\mu_3 & e^{Lk_4}\mu_4 & -e^{-Lk_4}\mu_4 \end{bmatrix} \tag{A.1}$$

$$[\mathbf{Q}] = \begin{bmatrix} p_{11} & p_{11} & p_{12} & p_{12} & p_{13} & p_{13} & p_{14} & p_{14} \\ p_{21} & -p_{21} & p_{22} & -p_{22} & p_{23} & -p_{23} & p_{24} & -p_{24} \\ p_{31} & p_{31} & p_{32} & p_{32} & p_{33} & p_{33} & p_{34} & p_{34} \\ p_{41} & p_{41} & p_{42} & p_{42} & p_{43} & p_{43} & p_{44} & p_{44} \\ -e^{Lk_1}p_{11} & -e^{-Lk_1}p_{11} & -e^{Lk_2}p_{12} & -e^{-Lk_2}p_{12} & -e^{Lk_3}p_{13} & -e^{-Lk_3}p_{13} & -e^{Lk_4}p_{14} & -e^{-Lk_4}p_{14} \\ -e^{Lk_1}p_{21} & e^{-Lk_1}p_{21} & -e^{Lk_2}p_{22} & e^{-Lk_2}p_{22} & -e^{Lk_3}p_{23} & e^{-Lk_3}p_{23} & -e^{Lk_4}p_{24} & e^{-Lk_4}p_{24} \\ -e^{Lk_1}p_{31} & -e^{-Lk_1}p_{31} & -e^{Lk_2}p_{32} & -e^{-Lk_2}p_{32} & -e^{Lk_3}p_{33} & -e^{-Lk_3}p_{33} & -e^{Lk_4}p_{34} & -e^{-Lk_4}p_{34} \\ -e^{Lk_1}p_{41} & -e^{-Lk_1}p_{41} & -e^{Lk_2}p_{42} & -e^{-Lk_2}p_{42} & -e^{Lk_3}p_{43} & -e^{-Lk_3}p_{43} & -e^{Lk_4}p_{44} & -e^{-Lk_4}p_{44} \end{bmatrix} \tag{A.2}$$

where

$$\begin{aligned} p_{1i} &= -k_i(EA\lambda_i - \beta k_i + \varepsilon_4\mu_i) \\ p_{2i} &= EI_w k_i^3 - \varepsilon_2 g_i k_i^2 + \gamma\omega^2 k_i - \lambda_i\left(\alpha\omega^2 + \beta\kappa_i^2\right) - \varepsilon_1\omega^2\mu_i \\ p_{3i} &= k_i(\beta\lambda_i - EI_w k_i + \varepsilon_2\mu_i) \\ p_{4i} &= -k_i\left(EI_\psi\mu_i + \varepsilon_2 k_i - \varepsilon_4\lambda_i\right) \end{aligned} \tag{A.3}$$

and λ_i and μ_i are given in Eq. (21).

Appendix B

The matrices $[\boldsymbol{M}_0]$, $[\boldsymbol{K}_0]$ $[\boldsymbol{M}_\mathrm{G}]$, $[\boldsymbol{K}_\mathrm{G}]$, $[\boldsymbol{C}_\mathrm{G}]$ and $[\boldsymbol{K}_\mathrm{C}]$ in Eq. (42) are defined as follows:

$$[M_0] = [M_{u\mathrm{b}}] + [M_{u\mathrm{v}}] + [M_{u\mathrm{p}}] + [M_{w\mathrm{b}}] + [M_{w\mathrm{v}}] + [M_{w\psi}] + [M_{w\mathrm{p}}] \tag{B.1}$$

where

$$[M_{u\mathrm{b}}] = \frac{\rho_\mathrm{b} A_\mathrm{b} L}{6}\begin{bmatrix} 2 & 0 & 0 & 0 & 1 & 0 & 0 & 0 \\ 0 & 0 & 0 & 0 & 0 & 0 & 0 & 0 \\ 0 & 0 & 0 & 0 & 0 & 0 & 0 & 0 \\ 0 & 0 & 0 & 0 & 0 & 0 & 0 & 0 \\ 1 & 0 & 0 & 0 & 2 & 0 & 0 & 0 \\ 0 & 0 & 0 & 0 & 0 & 0 & 0 & 0 \\ 0 & 0 & 0 & 0 & 0 & 0 & 0 & 0 \\ 0 & 0 & 0 & 0 & 0 & 0 & 0 & 0 \end{bmatrix} \tag{B.2}$$

$$[M_{uv}] = \frac{\rho_b A_b}{240}\begin{bmatrix} 80L & 60h_1 & -10Lh_1 & 40Lh_v & 40L & -60h_1 & 10Lh_1 & 20Lh_v \\ 60h_1 & 72h_1^2/L & 6h_1^2 & 30h_1h_v & 60h_1 & -72h_1^2/L & 6h_1^2 & 30h_1h_v \\ -10Lh_1 & 6h_1^2 & 8Lh_1^2 & -5Lh_1h_v & 10Lh_1 & -6h_1^2 & -2Lh_1^2 & 5Lh_1h_v \\ 40Lh_v & 30h_1h_v & -5Lh_1h_v & 20Lh_v^2 & 20Lh_v & -30h_1h_v & 5Lh_1h_v & 10Lh_v^2 \\ 40L & 60h_1 & 10Lh_1 & 20Lh_v & 80L & -60h_1 & -10Lh_1 & 40Lh_v \\ -60h_1 & -72h_1^2/L & -6h_1^2 & -30h_1h_v & -60h_1 & 72h_1^2/L & -6h_1^2 & -30h_1h_v \\ 10Lh_1 & 6h_1^2 & -2Lh_1^2 & 5Lh_1h_v & -10Lh_1 & -6h_1^2 & 8Lh_1^2 & -5Lh_1h_v \\ 20Lh_v & 30h_1h_v & 5Lh_1h_v & 10Lh_v^2 & 40Lh_v & -30h_1h_v & -5Lh_1h_v & 20Lh_v^2 \end{bmatrix} \tag{B.3}$$

$$[M_{up}] = \frac{\rho_p A_p}{120}\begin{bmatrix} 40L & 30h_2 & -5Lh_2 & 40Lh_v & 20L & -30h_2 & 5Lh_2 & 20Lh_v \\ -30h_2 & 36h_2^2/L & 3h_2^2 & 30h_2h_v & 30h_2 & -36h_2^2/L & 3h_2^2 & 30h_2h_v \\ 5Lh_2 & 3h_2^2 & 4Lh_2^2 & -5Lh_2h_v & 5Lh_2 & -3h_2^2 & -Lh_2^2 & 5Lh_2h_v \\ 40Lh_v & 30h_1h_v & -5Lh_1h_v & 40Lh_v^2 & 20Lh_v & -30h_1h_v & 5Lh_1h_v & 20Lh_v^2 \\ 20L & 30h_2 & 5Lh_2 & 20Lh_v & 40L & -30h_2 & -5Lh_2 & 40Lh_v \\ -30h_2 & -36h_2^2/L & -3h_2^2 & -30h_2h_v & -30h_2 & 36h_2^2/L & -3h_2^2 & -30h_2h_v \\ 5Lh_2 & 3h_2^2 & -Lh_2^2 & 5Lh_2h_v & -5Lh_2 & -3h_2^2 & 4Lh_2^2 & -5Lh_2h_v \\ 20Lh_v & 30h_1h_v & 5Lh_1h_v & 20Lh_v^2 & 40Lh_v & -30h_1h_v & -5Lh_1h_v & 40Lh_v^2 \end{bmatrix} \tag{B.4}$$

$$[M_{wb}] = \frac{\rho_b A_b L}{420}\begin{bmatrix} 140 & 0 & 0 & 0 & 70 & 0 & 0 & 0 \\ 0 & 156 & 22L & 0 & 0 & 54 & -13L & 0 \\ 0 & 22L & 4L^2 & 0 & 0 & 13L & -3L^2 & 0 \\ 0 & 0 & 0 & 0 & 0 & 0 & 0 & 0 \\ 70 & 0 & 0 & 0 & 140 & 0 & 0 & 0 \\ 0 & 54 & 13L & 0 & 0 & 156 & -22L & 0 \\ 0 & -13L & -3L^2 & 0 & 0 & -22L & 4L^2 & 0 \\ 0 & 0 & 0 & 0 & 0 & 0 & 0 & 0 \end{bmatrix} \tag{B.5}$$

$$[M_{wv}] = \frac{\rho_v A_v L}{420}\begin{bmatrix} 0 & 0 & 0 & 0 & 0 & 0 & 0 & 0 \\ 0 & 156 & 22L & 0 & 0 & 54 & -13L & 0 \\ 0 & 22L & 4L^2 & 0 & 0 & 13L & -3L^2 & 0 \\ 0 & 0 & 0 & 0 & 0 & 0 & 0 & 0 \\ 0 & 0 & 0 & 0 & 0 & 0 & 0 & 0 \\ 0 & 54 & 13L & 0 & 0 & 156 & -22L & 0 \\ 0 & -13L & -3L^2 & 0 & 0 & -22L & 4L^2 & 0 \\ 0 & 0 & 0 & 0 & 0 & 0 & 0 & 0 \end{bmatrix} \tag{B.6}$$

$$[M_{w\psi}] = \frac{\rho_v I_v}{420L}\begin{bmatrix} 0 & 0 & 0 & 0 & 0 & 0 & 0 & 0 \\ 0 & 504 & 42L & 210L & 0 & -504 & 42L & 210L \\ 0 & 42L & 56L^2 & -35L^2 & 0 & -42L & -14L^2 & 35L^2 \\ 0 & 210L & -35L^2 & 140L^2 & 0 & -210L & 35L^2 & 70L^2 \\ 0 & 0 & 0 & 0 & 0 & 0 & 0 & 0 \\ 0 & -504 & -42L & -210L & 0 & 504 & -42L & -210L \\ 0 & 42L & -14L^2 & 35L^2 & 0 & -42L & 56L^2 & -35L^2 \\ 0 & 210L & 35L^2 & 70L^2 & 0 & -210L & -35L^2 & 140L^2 \end{bmatrix} \tag{B.7}$$

$$[M_{wp}] = \frac{\rho_v A_v L}{420}\begin{bmatrix} 0 & 0 & 0 & 0 & 0 & 0 & 0 & 0 \\ 0 & 156 & 22L & 0 & 0 & 54 & -13L & 0 \\ 0 & 22L & 4L^2 & 0 & 0 & -13L & -3L^2 & 0 \\ 0 & 0 & 0 & 0 & 0 & 0 & 0 & 0 \\ 0 & 0 & 0 & 0 & 0 & 0 & 0 & 0 \\ 0 & 54 & 13L & 0 & 0 & 156 & -22L & 0 \\ 0 & -13L & -3L^2 & 0 & 0 & -22L & 4L^2 & 0 \\ 0 & 0 & 0 & 0 & 0 & 0 & 0 & 0 \end{bmatrix} \tag{B.8}$$

$$[K_0] = [K_{ub}] + [K_{uv}] + [K_{up}] + [K_{wb}] + [K_{wv}] + [K_{wp}] + [K_z] \tag{B.9}$$

where

$$[K_{ub}] = \frac{E_b A_b}{L}\begin{bmatrix} 1 & 0 & 0 & 0 & -1 & 0 & 0 & 0 \\ 0 & 0 & 0 & 0 & 0 & 0 & 0 & 0 \\ 0 & 0 & 0 & 0 & 0 & 0 & 0 & 0 \\ 0 & 0 & 0 & 0 & 0 & 0 & 0 & 0 \\ -1 & 0 & 0 & 0 & 1 & 0 & 0 & 0 \\ 0 & 0 & 0 & 0 & 0 & 0 & 0 & 0 \\ 0 & 0 & 0 & 0 & 0 & 0 & 0 & 0 \\ 0 & 0 & 0 & 0 & 0 & 0 & 0 & 0 \end{bmatrix} \tag{B.10}$$

$$[K_{uv}] = \frac{E_v A_v}{4L^3}\begin{bmatrix} 4L^2 & 0 & -2L^2h_1 & 2L^2h_v & -4L^2 & 0 & 2L^2h_1 & -2L^2h_v \\ 0 & 12h_1^2 & 6Lh_1^2 & 0 & 0 & -12h_1^2 & 6Lh_1^2 & 0 \\ -2L^2h_1 & 6Lh_1^2 & 4L^2h_1^2 & -L^2h_1h_v & 2L^2h_1 & -6Lh_1^2 & 2L^2h_1^2 & L^2h_1h_v \\ 2L^2h_v & 0 & -L^2h_1h_v & L^2h_v^2 & -2L^2h_v & 0 & L^2h_1h_v & -L^2h_v^2 \\ -4L^2 & 0 & 2L^2h_1 & -2L^2h_v & 4L^2 & 0 & -2L^2h_1 & 2L^2h_v \\ 0 & -12h_1^2 & -6Lh_1^2 & 0 & 0 & 12h_1^2 & -6Lh_1^2 & 0 \\ 2L^2h_1 & 6Lh_1^2 & 2L^2h_1^2 & L^2h_1h_v & -2L^2h_1 & -6Lh_1^2 & 4L^2h_1^2 & -L^2h_1h_v \\ -2L^2h_v & 0 & L^2h_1h_v & -L^2h_v^2 & 2L^2h_v & 0 & -L^2h_1h_v & -L^2h_v^2 \end{bmatrix} \tag{B.11}$$

$$[K_{up}] = \frac{E_p A_p}{2L^3}\begin{bmatrix} 2L^2 & 0 & -L^2h_2 & 2L^2h_v & -2L^2 & 0 & L^2h_2 & -2L^2h_v \\ 0 & 6h_2^2 & 3Lh_2^2 & 0 & 0 & -6h_2^2 & 3Lh_2^2 & 0 \\ -L^2h_2 & 3Lh_2^2 & 2L^2h_2^2 & -L^2h_2h_v & L^2h_2 & -3Lh_2^2 & L^2h_2^2 & L^2h_2h_v \\ 2L^2h_v & 0 & -L^2h_2h_v & 2L^2h_v^2 & -2L^2h_v & 0 & L^2h_2h_v & -2L^2h_v^2 \\ -2L^2 & 0 & L^2h_2 & -2L^2h_v & 2L^2 & 0 & -L^2h_2 & 2L^2h_v \\ 0 & -6h_2^2 & -3Lh_2^2 & 0 & 0 & 6h_2^2 & -3Lh_2^2 & 0 \\ L^2h_2 & 3Lh_2^2 & L^2h_2^2 & L^2h_2h_v & -L^2h_2 & -3Lh_2^2 & 2L^2h_2^2 & -L^2h_2h_v \\ -2L^2h_v & 0 & L^2h_2h_v & -2L^2h_v^2 & 2L^2h_v & 0 & -L^2h_2h_v & 2L^2h_v^2 \end{bmatrix} \tag{B.12}$$

$$[K_{wb}] = \frac{E_b I_b}{L^3}\begin{bmatrix} 0 & 0 & 0 & 0 & 0 & 0 & 0 & 0 \\ 0 & 12 & 6L & 0 & 0 & -12 & 6L & 0 \\ 0 & 6L & 4L^2 & 0 & 0 & -6L & 2L^2 & 0 \\ 0 & 0 & 0 & 0 & 0 & 0 & 0 & 0 \\ 0 & 0 & 0 & 0 & 0 & 0 & 0 & 0 \\ 0 & -12 & -6L & 0 & 0 & 12 & -6L & 0 \\ 0 & 6L & 2L^2 & 0 & 0 & -6L & 4L^2 & 0 \\ 0 & 0 & 0 & 0 & 0 & 0 & 0 & 4L^2 \end{bmatrix} = \frac{E_b I_b}{L^3}[K_w] \tag{B.13}$$

$$[K_{wv}] = \frac{E_v I_v}{L^3}\begin{bmatrix} 0 & 0 & 0 & 0 & 0 & 0 & 0 & 0 \\ 0 & 12 & 6L & 0 & 0 & -12 & 6L & 0 \\ 0 & 6L & 4L^2 & -L^2 & 0 & -6L & 2L^2 & L^2 \\ 0 & 0 & -L^2 & L^2 & 0 & 0 & L^2 & -L^2 \\ 0 & 0 & 0 & 0 & 0 & 0 & 0 & 0 \\ 0 & -12 & -6L & 0 & 0 & 12 & -6L & 0 \\ 0 & 6L & 2L^2 & L^2 & 0 & -6L & 4L^2 & -L^2 \\ 0 & 0 & L^2 & -L^2 & 0 & 0 & -L^2 & L^2 \end{bmatrix} \tag{B.14}$$

$$[K_{wp}] = \frac{E_p A_p}{L^3}[K_w] \tag{B.15}$$

$$[K_z] = A_v \kappa(1+\alpha)\begin{bmatrix} 0 & 0 & 0 & 0 & 0 & 0 & 0 & 0 \\ 0 & 0 & 0 & 0 & 0 & 0 & 0 & 0 \\ 0 & 0 & 0 & 0 & 0 & 0 & 0 & 0 \\ 0 & 0 & 0 & 2 & 0 & 0 & 0 & 1 \\ 0 & 0 & 0 & 0 & 0 & 0 & 0 & 0 \\ 0 & 0 & 0 & 0 & 0 & 0 & 0 & 0 \\ 0 & 0 & 0 & 0 & 0 & 0 & 0 & 0 \\ 0 & 0 & 0 & 1 & 0 & 0 & 0 & 2 \end{bmatrix} \tag{B.16}$$

$$[M_G] = \frac{A_v \alpha \kappa L}{6\hat{\omega}^2}\begin{bmatrix} 2 & 1 \\ 1 & 2 \end{bmatrix} \tag{B.17}$$

$$[K_G] = \frac{A_v \alpha \kappa L}{6}\begin{bmatrix} 2 & 1 \\ 1 & 2 \end{bmatrix} \tag{B.18}$$

$$[C_G] = \frac{A_v \alpha \kappa \hat{\zeta} L}{3\hat{\omega}}\begin{bmatrix} 2 & 1 \\ 1 & 2 \end{bmatrix} \tag{B.19}$$

$$[K_C] = \frac{A_v \alpha \kappa L}{6}\begin{bmatrix} 0 & 0 & 0 & 0 & 0 & 0 & 0 & 0 & 0 & 0 \\ 0 & 0 & 0 & 0 & 0 & 0 & 0 & 0 & 0 & 0 \\ 0 & 0 & 0 & 0 & 0 & 0 & 0 & 0 & 0 & 0 \\ 0 & 0 & 0 & 0 & 0 & 0 & 0 & 0 & -2 & -1 \\ 0 & 0 & 0 & 0 & 0 & 0 & 0 & 0 & 0 & 0 \\ 0 & 0 & 0 & 0 & 0 & 0 & 0 & 0 & 0 & 0 \\ 0 & 0 & 0 & 0 & 0 & 0 & 0 & 0 & 0 & 0 \\ 0 & 0 & 0 & 0 & 0 & 0 & 0 & 0 & -1 & -2 \\ 0 & 0 & 0 & -2 & 0 & 0 & 0 & -1 & 0 & 0 \\ 0 & 0 & 0 & -1 & 0 & 0 & 0 & -2 & 0 & 0 \end{bmatrix} \tag{B.20}$$

References

Banerjee, J.R., 1997. Dynamic stiffness formulation for structural elements: a general approach. Computers and Structures 63 (1), 101–103.

Baz, A., 1993. Active constrained layer damping. Proc. Damping'93, San Francisco, CA. November, 1993. pp. IBB 1–23.

Cheng, Z.Q., Lim, C.W., Kitipornchai, S., 1999. Three-dimensional exact solution for inhomogeneous and laminated piezoelectric plates. International Journal of Engineering Science 37 (11), 1425–1439.

Cheng, Z.Q., Lim, C.W., Kitipornchai, S., 2000. Three-dimensional asymptotic approach for inhomogeneous and laminated piezoelectric plates. International Journal of Solids and Structures 37 (23), 3153–3175.

Christensen, R.M., 1982. Theory of Viscoelasticity: an Introduction, second ed. Academic Press, New York.

Crawley, E.F., de Luis, J., 1987. Use of piezoelectric actuators as elements of intelligent structures. AIAA Journal 25 (10), 1373–1385.

DiTaranto, R.A., 1965. Theory of vibratory bending for elastic and viscoelastic layered finite length beams. Journal of Applied Mechanics 87, 881–887.

Doyle, J.F., 1988. A spectrally formulated finite element for longitudinal wave propagation. International Journal of Analytical and Experimental Modal Analysis 3, 1–5.

Hess, M.S., 1969. The end problem for a laminated elastic strip-I the general solution. Journal of Composite Materials 3, 262–280.

Kerwin, E.M., 1959. Damping of flexural waves by a constrained viscoelastic layer. Journal of Acoustical Society of America 31 (7), 952–962.

Lam, M.J., Saunders, W.R., Inman, D.J., 1995. Modeling active constrained layer damping using Golla-Hughes-McTavish approach. Proc. Conference on Smart Structures and Materials: Passive Damping, San Diego, CA. March 1995, SPIE vol. 2445, pp. 86–97.

Lee, U., Kim, J., 1998. Spectral element modeling of piezoelectric layered beams. Proc. Fourth International Conference on Motion and Vibration Control, Zurich, Switzerland, August 1998, vol. 1, pp. 267–272.

Lee, U., Kim, J., 2000a. Determination of non-ideal beam boundary conditions: a spectral element approach. AIAA Journal 38 (2), 309–316.

Lee, U., Kim, J., 2000b. Dynamics of elastic-piezoelectric two-layer beams using spectral element method. International Journal of Solids and Structures 37 (32), 4403–4417.

Lee, U., Lee, J., 1997. Dynamic analysis of one and two-dimensional structures using spectral element methods. Proc. Sixth International Conference on Recent Advances in Structural Dynamics ISVR, University of Southampton, pp. 263–277.

Lee, U., 1998. Equivalent continuum representation of lattice beams: spectral element approach. Engineering Structures 20 (7), 587–592.

Lee, U., 1999. Spectral element method for levy-type plates subject to dynamic loads. Journal of Engineering Mechanics 125 (2), 243–247.

Leibowitz, M.M., Vinson, J.R., 1993. On active (piezoelectric) constrained layer damping in composite sandwich structures. Proc. Fourth International Conference on Adaptive Structures Cologne, Germany, pp. 530–541.

Lesieutre, G.A, Lee, U., 1996. A finite element for beams having segmented active constrained layers with frequency-dependent viscoelastics. Smart Structures and Materials 5, 615–627.

Leung, A.Y.T., 1993. Dynamic Stiffness and Substructures Springer, London.

Leung, A.Y.T., Zhou, W.E., 1996. Dynamic stiffness analysis of laminated composite plates. Thin-Walled Structures 25 (2), 109–133.

Liao, W.H., 1997. Active-passive hybrid structural control: an enhanced active constrained layer damping treatment with edge elements. Ph.D. Thesis, The Pennsylvania State University, PA.

Liao, W.H., 2000. Private Communication.

McTavish, D.J., Hughes, P.C., 1993. Modeling of linear viscoelastic space structures. Journal of Vibration and Acoustics 115, 103–110.

Mead, D.J., Markus, S., 1969. The forced vibration of a three-layer, damped sandwich beam with arbitrary boundary conditions. Journal of Sound and Vibration 10 (2), 163–175.

Nath, S., Wereley, N.M., 1995. Active constrained layer damping for rotorcraft flex beams. Proc. 34th AIAA/ASME/ASCE/AHS/ASC Structures, Structural Dynamics, and Materials Conference New Orleans, LA. April 1995, pp. 2867–2875.

Oberst, H., 1952. Uber die dampfung der biege-schwinggungen dunner bleche durch fest haftende belage. Acusta 2, 181–194.

Plump, J.M., Hubbard, J.E. Jr., 1986. Modeling of an active constrained layer damper. Proc. 12th International Congress on Acoustics, Toronto, Canada, July 1986, Paper no. D4-1.

Shen, I.Y., 1994. Hybrid damping through intelligent constrained layer treatments. Journal of Vibration and Acoustics 116, 341–349.

Soovere, J., Drake, M.L., 1985. Aerospace Structures Technology Damping Design Guide, Volume III – Damping Material Data, AFWAL-TR-84-3089.

Timoshenko, S., 1925. Analysis of bi-metal thermostats. Journal of Optical Society of America 11, 233–256.

Wang, G., Wereley, N.M., 1998. Frequency response of beams with passively constrained damping layers and piezo-actuators. Proc. Fifth SPIE Symposium on Smart Structures and Materials, Passive Damping and Isolation Conference San Diego, CA, March 1998, Paper no. 3327-05, pp. 44–60.

Wolfram, S., 1996. The Mathematica Book, third ed. Wolfram Media, Cambridge University Press, Cambridge, MA.

Yan, M.J., Dowell, E.H., 1972. Governing equations for vibrating constrained-layer damping sandwich plates and beams. Journal of Applied Mechanics 39, 1041–1046.